

REPORT

GRAVITATION

Relativistic redshift of the star S0-2 orbiting the Galactic Center supermassive black hole

Tuan Do^{1*}, Aurelien Hees^{2,1}, Andrea Ghez¹, Gregory D. Martinez¹, Devin S. Chu¹, Siyao Jia³, Shoko Sakai¹, Jessica R. Lu³, Abhimat K. Gautam¹, Kelly Kosmo O'Neil¹, Eric E. Becklin^{1,4}, Mark R. Morris¹, Keith Matthews⁵, Shogo Nishiyama⁶, Randy Campbell⁷, Samantha Chappell¹, Zhuo Chen¹, Anna Ciurlo¹, Arezu Dehghanfar^{1,8}, Eulalia Gallego-Cano⁹, Wolfgang E. Kerzendorf^{10,11,12,13}, James E. Lyke⁷, Smadar Naoz^{1,14}, Hiromi Saida¹⁵, Rainer Schödel⁹, Masaaki Takahashi¹⁶, Yohsuke Takamori¹⁷, Gunther Witzel^{1,18}, Peter Wizinowich⁷

The general theory of relativity predicts that a star passing close to a supermassive black hole should exhibit a relativistic redshift. In this study, we used observations of the Galactic Center star S0-2 to test this prediction. We combined existing spectroscopic and astrometric measurements from 1995–2017, which cover S0-2's 16-year orbit, with measurements from March to September 2018, which cover three events during S0-2's closest approach to the black hole. We detected a combination of special relativistic and gravitational redshift, quantified using the redshift parameter Υ . Our result, $\Upsilon = 0.88 \pm 0.17$, is consistent with general relativity ($\Upsilon = 1$) and excludes a Newtonian model ($\Upsilon = 0$) with a statistical significance of 5σ .

General relativity (GR) has been thoroughly tested in weak gravitational fields in the Solar System (1), with binary pulsars (2) and with measurements of gravitational waves from stellar-mass black hole binaries (3, 4). Observations of short-period stars in our Galactic Center (GC) (5–8) allow GR to be tested in a different regime (9): the strong field near a supermassive black hole (SMBH) (10, 11). The star S0-2 (also known as S2) has a 16-year orbit around Sagittarius A* (Sgr A*), the SMBH at the center of the Milky Way. In 2018 May, S0-2 reached its point of closest approach, at a distance of 120 astronomical units with a velocity reaching 2.7% of the speed of light. Within a 6-month interval of that date, the star also passed through its maximum and minimum velocity (in March and September, respectively) along the line of sight, spanning 6000 km s^{-1} in radial velocity (RV) (Fig. 1). Here we present observations of all three events combined with data from 1995–2017 (Fig. 2).

During 2018, the close proximity of S0-2 to the SMBH caused the relativistic redshift, which is the combination of the transverse Doppler shift from special relativity and the gravitational redshift from GR. This deviation from a Keplerian orbit was predicted to reach 200 km s^{-1} (Fig. 3) and is detectable with current telescopes. The GRAVITY collaboration (9) previously reported a similar measurement. Our measurements are complementary in the following ways: (i) We took a complete set of independent measurements with three additional months of data, doubling the time baseline for the year of closest approach and including the third turning point (RV minimum) in September 2018. (ii) We used three different spectroscopic instruments in 2018, enabling us to probe the presence of instrumental biases. (iii) To test for bias in the result, we analyzed the systematic errors that may arise from an experiment spanning more than 20 years. (iv) We publicly released the stellar measurements and the posterior probability distributions.

We used a total of 45 astrometric positional measurements (spanning 24 years) and 115 RVs (18 years) to fit the orbit of S0-2. Of these, 11 are new astrometric measurements of S0-2 from 2016 to 2018 and 28 are new RV measurements from 2017 and 2018 (Fig. 1). Astrometric measurements were obtained at the W. M. Keck Observatory by using speckle imaging (a technique to overcome blurring from the atmosphere by taking very short exposures and combining the images with software) from 1995–2005 and adaptive optics (AO) imaging (12) from 2005–2018. RV measurements were obtained from the W. M. Keck Observatory, Gemini North Telescope, and Subaru Telescope. All of our RV observations were taken using AO. We supplement our observations with previously reported RVs from Keck from 2000 (7) and the Very Large Telescope from 2003–2016 (8). This work includes data from two imaging instruments and six spectroscopic instruments (13).

We scheduled our 2018 observations using a tool designed to maximize the sensitivity of the experiment to the redshift signal (13). We predicted that, given the existing data (1995–2017), spectroscopic measurements at the RV maximum and minimum in 2018 would provide the most sensitivity and thus would be ideal for detecting the relativistic redshift (Fig. 3). Although they are less sensitive to the effect of the redshift, imaging observations of the sky position of S0-2 in 2018 also slightly improve the measurement of the relativistic redshift.

The RVs of S0-2 are measured by fitting a physical model (which includes properties of the star, such as its effective temperature, surface gravity, and rotational velocity in addition to RV) to its observed spectrum (13). The same procedure is applied to the new and archival observations; for the latter, this spectroscopic method improves the precision by a factor of 1.7 compared with previous analyses (14, 15).

We also characterized additional sources of uncertainties beyond the uncertainties in the fitted model. (i) The wavelength solution, which transforms locations on the detector to vacuum wavelengths, was characterized by comparing the observed wavelengths of atmospheric OH emission lines in the spectra of S0-2 and in observations of blank sky to their known vacuum wavelengths. This comparison shows the uncertainty of the wavelength solution of the spectroscopic instruments to be $\sim 2 \text{ km s}^{-1}$, with some observations from 2002–2004 having lower accuracy between 2 and 26 km s^{-1} . (ii) Reexamination

¹Department of Physics and Astronomy, University of California, Los Angeles, CA 90095, USA. ²Systèmes de Référence Temps Espace, Observatoire de Paris, Université Paris-Sciences-et-Lettres, Centre National de la Recherche Scientifique, Sorbonne Université, Laboratoire National de Métrologie et d'Essais, 61 Avenue de l'Observatoire, 75014 Paris, France. ³Department of Astronomy, University of California, Berkeley, CA 94720, USA. ⁴Universities Space Research Association/Stratospheric Observatory for Infrared Astronomy, NASA Ames Research Center, Mail Stop N232-12, Moffett Field, CA 94035, USA. ⁵Division of Physics, Mathematics, and Astronomy, California Institute of Technology, MC 301-17, Pasadena, CA 91125, USA. ⁶Faculty of Education, Miyagi University of Education, 149 Aramaki-aza-aoba, Aoba-ku, Sendai, Miyagi 980-0845, Japan. ⁷W. M. Keck Observatory, 65-1120 Mamalahoa Highway, Kamuela, HI 96743, USA. ⁸Institut de Planétologie et d'Astrophysique de Grenoble, 414 Rue de la Piscine, 38400 Saint-Martin-d'Hères, France. ⁹Instituto de Astrofísica de Andalucía, Consejo Superior de Investigaciones Científicas, Glorieta de la Astronomía S/N, 18008 Granada, Spain. ¹⁰European Southern Observatory, Karl-Schwarzschild-Straße 2, 85748 Garching bei München, Germany. ¹¹Center for Cosmology and Particle Physics, New York University, 726 Broadway, New York, NY 10003, USA. ¹²Department of Physics and Astronomy, Michigan State University, East Lansing, MI 48824, USA. ¹³Department of Computational Mathematics, Science, and Engineering, Michigan State University, East Lansing, MI 48824, USA. ¹⁴Mani L. Bhaumik Institute for Theoretical Physics, Department of Physics and Astronomy, University of California, Los Angeles, CA 90095, USA. ¹⁵Faculty of Liberal Arts, Daido University, 10-3 Takiharuro-cho, Minami-ku, Nagoya, Aichi 457-8530, Japan. ¹⁶Department of Physics and Astronomy, Aichi University of Education, 1 Hirotsawa, Igaya-cho, Kariya, Aichi 448-8542, Japan. ¹⁷National Institute of Technology, Wakayama College, 77 Noshima, Nada-cho, Gobo, Wakayama 644-0023, Japan. ¹⁸Max Planck Institute for Radio Astronomy, Auf dem Hügel 69, D-53121 Bonn, Germany.

*Corresponding author. Email: tdo@astro.ucla.edu

of the spectroscopic data showed that one spectroscopic instrument [Near-Infrared Camera 2 (NIRC2)] had additional systematic bias from its optical system, which resulted in a systematic offset in RV compared with other instruments.

We include an RV offset parameter in the orbit fit to account for this systematic offset. (iii) We assessed systematic uncertainty by observing bright RV standard stars of the same spectral-type as S0-2 (table S3). This systematic

error is $1.3 \pm 1.2 \text{ km s}^{-1}$, smaller than the statistical uncertainties and $\sim 17\%$ of previous RV measurements of S0-2 (15). When these sources of systematic error are included in the analysis, the average RV uncertainty of S0-2 is

Fig. 1. Spectroscopy and imaging of the star S0-2.

(A) Weighted-average spectrum of S0-2 from data obtained during 2006–2018 at the Keck Observatory. The strongest feature, which provides most of the RV constraint, is from the H I line at $2.1661 \mu\text{m}$. (B) Sequence of S0-2 spectra observed in 2017 and 2018 (black lines). The RV of the star changes by more than 6000 km s^{-1} throughout 2018. The dashed line shows the rest wavelength of the H I line. We fit a model to the spectrum that simultaneously constrains the star’s physical properties, such as effective temperature and rotation, along with the RV of the star (orange lines). This model accounts for the asymmetries in the H I feature. (C) Inverted Keck AO image of S0-2 (center of image) from March 2018 with the H-band filter ($1.6 \mu\text{m}$).

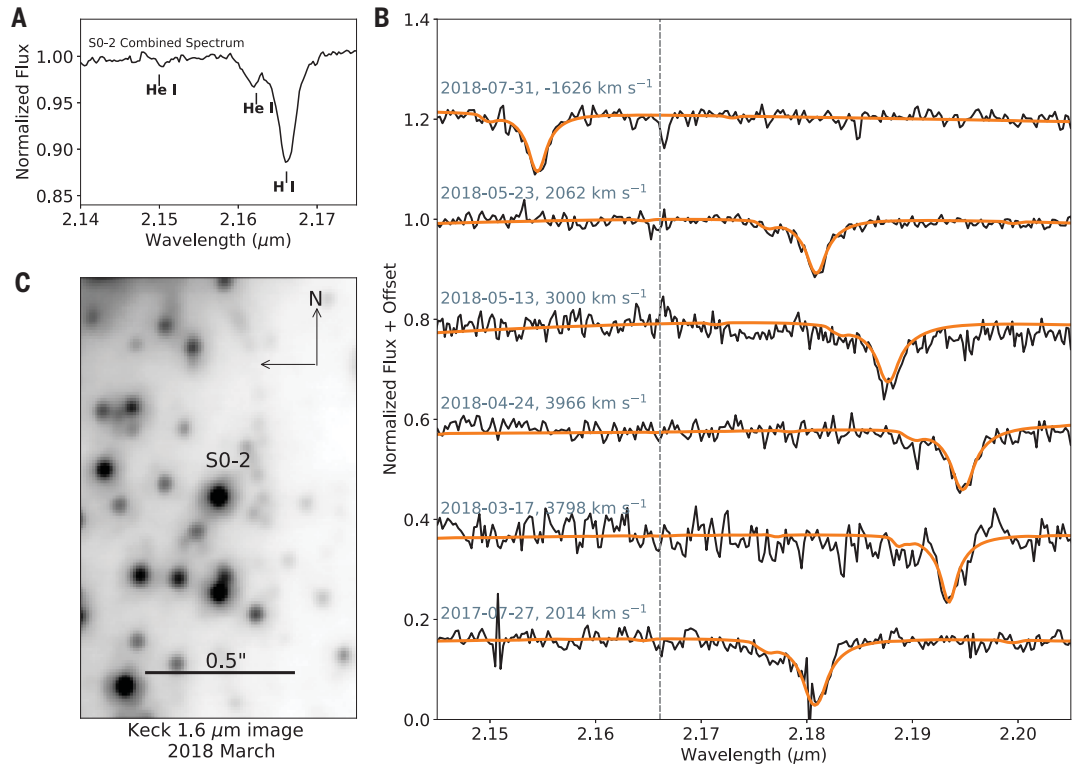
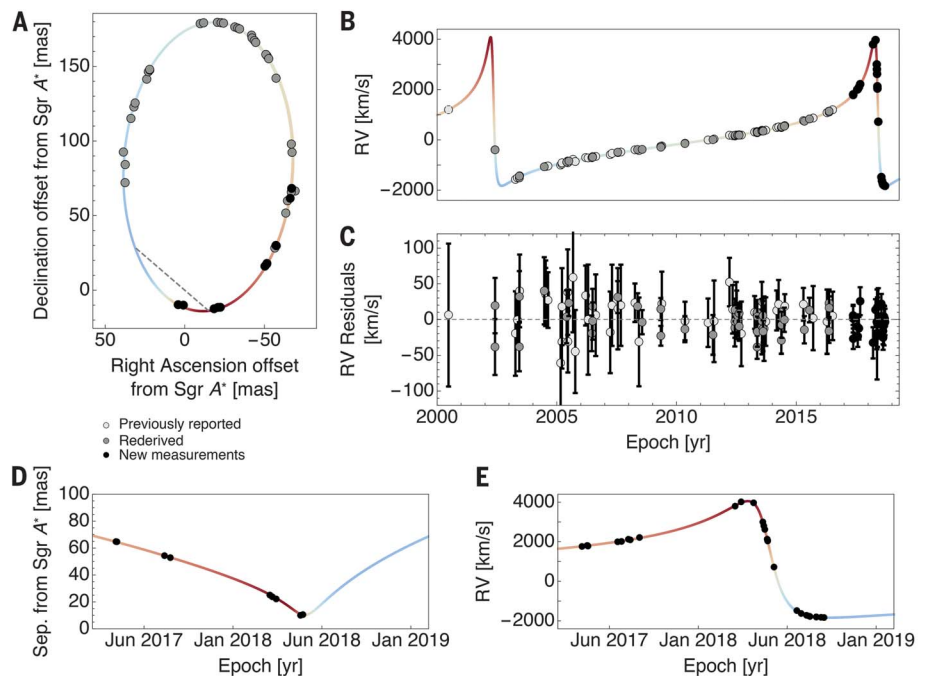


Fig. 2. GR orbit modeling of S0-2. (A) Astrometric measurements of the short-period star S0-2 in orbit around the SMBH Sgr A*, overlaid with our best-fitting projected orbit in the plane of the sky. The origin of the coordinate system coincides with the fitted SMBH center of mass (13). The x and y axes correspond to offsets in right ascension and declination, respectively, from the SMBH. We used 45 astrometric measurements from 1995–2018, of which 11 are new observations (black circles) and 34 are rederived measurements (dark gray circles). The best-fitting SMBH linear drift has been removed from the measurements. The line of nodes (dashed line) shows the intersection of the orbital plane with the plane of the sky (this line also passes through the position of the black hole). S0-2 moves clockwise in this projection; the star is behind the black hole below the line of nodes and in front of the black hole above the line of nodes. The color and intensity used in the best-fitting orbital plot represent the direction and magnitude of the line-of-sight velocity, with colors corresponding to those in (B). (B) RV measurements and the best-fitting RV model (colored line) using 115 RV measurements from 2000–2018. Forty-two measurements were previously reported (light gray circles), 45 were rederived for this work with improved methodology (dark gray circles), and 28 are new observations (black circles). The color of the best-fitting orbit represents the value and sign of the line-of-sight velocity. (C) Residuals from the best-fitting RV model. Error bars indicate 1σ uncertainties. (D and E) Observations around the three turning points, one at the closest approach to Sgr A* in the plane of the sky (D) and two RV turning points (maximum and minimum RV) (E), provide the greatest sensitivity to the relativistic redshift.



found to be 20 km s^{-1} for the Keck and Gemini observations.

The astrometric positions of S0-2 with respect to Sgr A* were placed in a common absolute astrometric reference frame by using a multistep

cross-matching and transformation process. We adopted an improved methodology for obtaining precise astrometry and a more accurate absolute reference frame compared with that of previous work (7). This resulted in an average astromet-

ric uncertainty for S0-2 of 1.1 milli-arc seconds (mas) for speckle imaging and 0.26 mas for AO imaging.

The astrometric and RV measurements are combined in a global orbital model fitting using a standard post-Newtonian approximation that includes the first-order GR corrections on the Newtonian equations of motion, the Römer time delay due to variations in the light propagation time between S0-2 and the observer, and the relativistic redshift. For the astrometric observables, we ignore the negligible effect of light deflection by the SMBH but include a two-dimensional (2D) linear drift of the gravitational center of mass. This drift accounts for systematic uncertainties in the construction of the astrometric reference frame. To our level of accuracy, the RV observable is (13)

$$RV = v_{z_0} + V_{Z,S0-2} + \Upsilon \left[\frac{V_{S0-2}^2}{2c} + \frac{GM}{cR_{S0-2}} \right] \quad (1)$$

where c is the speed of light in a vacuum, v_{z_0} is a constant offset introduced to account for systematic uncertainties within our RV reduction, $V_{Z,S0-2}$ is the Newtonian line-of-sight velocity of S0-2, $V_{S0-2}^2/2c$ is the transverse Doppler shift predicted by special relativity depending on S0-2's velocity \mathbf{V}_{S0-2} , and GM/cR_{S0-2} is the gravitational redshift predicted by GR incorporating the SMBH gravitational parameter GM (gravitational constant G and SMBH mass M) and the distance, R_{S0-2} , between S0-2 and the SMBH. Υ is a scale parameter introduced to characterize deviations from GR; its value is 0 in a purely Newtonian model and 1 in GR (13). The model has 14 parameters: 6 orbital parameters for S0-2, the gravitational parameter of the SMBH (GM), the distance to the GC R_0 , a 2D linear drift of the SMBH parametrized by the 2D position (x_0, y_0) and velocity (v_{x_0}, v_{y_0}) of the black hole from the

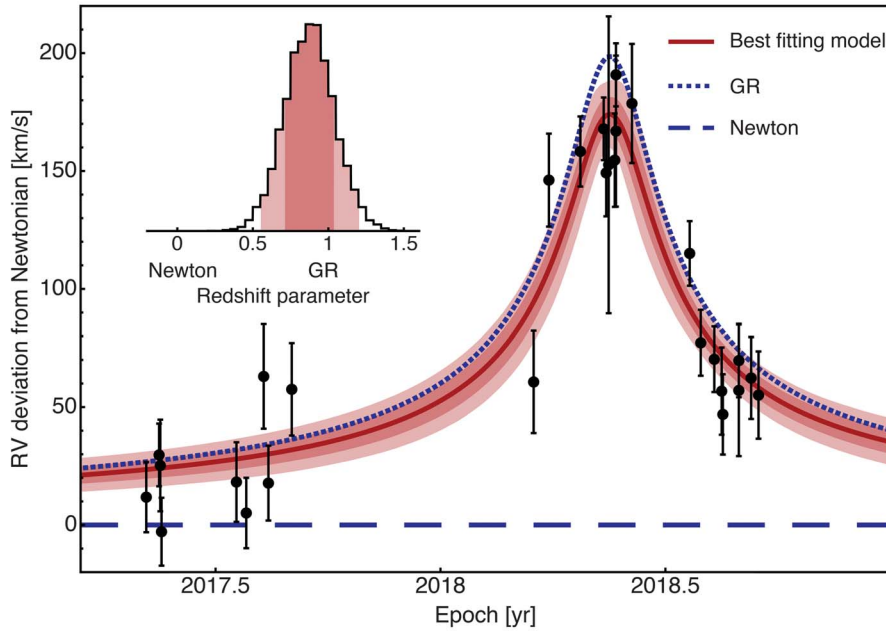


Fig. 3. Measured deviation from Newtonian predictions. The fitted deviation from Newtonian predictions, overlaid with the best-fitting orbit model (red line) corresponding to $\Upsilon = 0.88$. The inset shows the posterior probability distribution for Υ ; 0.88 is the median value. The red shaded areas show the model 68 and 95% confidence intervals. The observed RVs are shown as black circles, after removing the Newtonian part of the model. Error bars indicate 1σ uncertainties. For comparison, we show the RV deviation expected for a purely relativistic signal ($\Upsilon = 1$, dotted blue line) and for a purely Newtonian model ($\Upsilon = 0$, dashed blue line) for an orbit with the same orbital parameters. Our measurement is consistent with the GR model at the 1σ confidence level, whereas the Newtonian model is excluded at $>5\sigma$ confidence.

Table 1. Estimation of the model parameters. Column four (Estimation) indicates the median of the marginalized 1D posterior. Column five (Statistical uncertainty) indicates the half width of the 68% confidence interval centered on the median. Values for λ denote the $+1\sigma$ and -1σ uncertainties. Column six (Systematic σ from jackknife) indicates the 1σ systematic uncertainty from the reference frame estimated from the jackknife analysis (13). M_\odot , solar mass.

Parameter	Description	Maximum likelihood	Estimation	Statistical uncertainty	Systematic σ from jackknife
$M_{\text{BH}} (10^6 M_\odot)$	Black hole mass	3.984	3.975	0.058	0.026
R_0 (kpc)	Distance to GC	7.971	7.959	0.059	0.032
Υ	Redshift parameter	0.80	0.88	0.16	0.047
x_0 (mas)	x dynamical center	0.99	1.22	0.32	0.51
y_0 (mas)	y dynamical center	-0.85	-0.88	0.34	1.16
v_{x_0} (mas/year)	x velocity	-0.060	-0.077	0.018	0.14
v_{y_0} (mas/year)	y velocity	0.221	0.226	0.019	0.066
v_{z_0} (km/s)	z velocity	-3.6	-6.2	3.7	0.79
P (years)	Period	16.041	16.042	0.0016	7.8×10^{-5}
T_0 (years)	Closest approach	2018.3765	2018.3763	0.0004	1.9×10^{-5}
e	Eccentricity	0.886	0.8858	0.0004	2.8×10^{-5}
i (degrees)	Inclination	133.88	133.82	0.18	0.13
ω (degrees)	Argument of periapsis	66.03	66.11	0.24	0.077
Ω (degrees)	Angle to the ascending node	227.40	227.49	0.29	0.11
NIRC2 offset (km/s)	RV offset	80	81	19	0.8
Λ (mas)	Astrometric correlation length	21	28	$^{24.6}_{-13.6}$	11.8
p	Astrometric mixing coefficient	0.47	0.55	0.13	0.11

center of the reference frame, an offset for the RV v_{z_0} , and the redshift parameter Υ .

Several statistical tests were performed to assess systematic effects, using two different information criteria estimators—the Bayesian evidence and the expected logarithm predicted density—to compare models (13). We examined several sources of systematic uncertainties in the orbital fit: (i) potential offsets in RVs and astrometric positions from different instruments and (ii) potentially correlated uncertainties in astrometric measurements. On the basis of Bayesian model selection, we find that one spectrograph requires an RV offset with respect to other instruments (likely due to optical fringing) (13). No other instruments require an RV or astrometric positional offset. We include a parameter for the spectrograph RV offset in the model so it is fitted simultaneously. On the basis of the model selection criteria, we also find spatial correlation in the astrometric uncertainties. The correlated uncertainties are modeled with a multivariate likelihood characterized by a covariance matrix. The correlation matrix introduces a characteristic correlation length scale Λ and a mixing parameter p , both of which are simultaneously fitted with the model parameters (13). We validated this approach via Monte Carlo analysis, by randomly choosing one astrometric measurement per length scale to empirically estimate the effect of correlation scales. Although the inclusion of these systematic effects does not significantly affect the best-fitting Υ value, it increases the uncertainties, influencing the precision of the results.

We developed an orbit modeling software package to model the orbits. The software employs Bayesian inference for model fitting, using nested sampling to estimate the posterior probability distribution via the multinest package (16, 17). We also performed Monte Carlo simulations to evaluate our fitting methodology and show that the statistical uncertainties are robust (13).

We initially compared a purely Newtonian model with a purely relativistic (Υ fixed to 1) model. We used the Bayes factor model selection criterion to show that the relativistic model is preferred by the data, with high confidence. The difference of the logarithm of the Bayesian evidence between these two models is 10.68. Expressed as an odds ratio, the GR model is 43,000 times more likely than the Newtonian model in explaining the observations.

We then fitted the more general model that includes the Υ redshift parameter as a free parameter. The estimated values for the 17 fitted parameters are in Table 1 (the posterior distributions are shown in figs. S10 to S13). The estimation $\Upsilon = 0.88 \pm 0.16$ and its marginal posterior is shown in Fig. 3C. We estimated the systematic uncertainties due to the astrometric reference frame construction by performing a jackknife analysis on stars used to construct the reference frame. This adds a systematic uncertainty on the redshift parameter of ~ 0.047 , which, when added in quadrature with the statistical uncertainties, results in a total uncertainty $\sigma_{\Upsilon} = 0.17$.

The measured redshift parameter is therefore 0.88 ± 0.17 , consistent with GR at the 1 σ level, whereas the Newtonian value $\Upsilon = 0$ is excluded by $>5\sigma$. Our estimation also agrees at the 1 σ level with the measurement by the GRAVITY collaboration (9). Our experiment is independent from theirs, using a different set of measurements that includes the third turning point. We examined additional sources of systematic error that were previously not considered. The best-fitting model to the RV and the fit residuals is presented in Fig. 2. A fit using a parameter encoding deviations from GR only at the level of the gravitational redshift gives $\alpha = -0.24 \pm 0.32$, where $\alpha = 2(\Upsilon - 1)$ is the standard gravitational redshift parameter (1, 13).

Our observations also constrain two other parameters: the mass of the black hole (M_{BH}) and the distance to the GC (R_0). From our model with Υ as free parameter, the 68% marginalized confidence interval for $M_{\text{BH}} = (3.984 \pm 0.058 \pm 0.026) \times 10^6 M_{\odot}$ and $R_0 = 7971 \pm 59 \pm 32$ pc, where the first uncertainty is the statistical uncertainty and the second uncertainty is the systematic error σ from the jackknife analysis (Table 1). If we assume GR is true, then $M_{\text{BH}} = (3.964 \pm 0.047 \pm 0.026) \times 10^6 M_{\odot}$ and $R_0 = 7946 \pm 50 \pm 32$ pc (see supplementary text for discussion). The nested sampling chains are provided in data S3.

The gravitational redshift is a direct consequence of the universality of free fall and of special relativity (18), and hence of the Einstein equivalence principle, a fundamental principle of GR that provides a geometric interpretation for gravitational interactions. Violations of the equivalence principle are predicted by some theories of modified gravity motivated by the development of a quantum theory of gravitation, unification theories, and some models of dark energy (19). Although the gravitational redshift has been measured with higher precision within the Solar System (20, 21), our results and those of the GRAVITY collaboration (9) extend the measurements to higher gravitational redshift and around a massive compact object, a SMBH. Sgr A* has a mass $\sim 4 \times 10^6$ times that of the Sun. This constrains modified theories of gravitation that exhibit large nonperturbative effects around black holes but not around non-compact objects such as those in the Solar System [see (22–24) and supplementary text]. This redshift test is also performed in an environment that differs from the Solar System, where some theories predict modifications of GR to be screened or hidden (25).

REFERENCES AND NOTES

1. C. M. Will, *Living Rev. Relativ.* **17**, 4 (2014).
2. M. Kramer, *Int. J. Mod. Phys. D* **25**, 1630029 (2016).
3. B. P. Abbott et al.; LIGO Scientific and Virgo Collaborations, *Phys. Rev. Lett.* **116**, 221101 (2016).
4. B. P. Abbott et al., *Astrophys. J.* **848**, L13 (2017).
5. R. Genzel, N. Thatte, A. Krabbe, H. Kroker, L. E. Tacconi-Garman, *Astrophys. J.* **472**, 153–172 (1996).
6. A. M. Ghez, B. L. Klein, M. Morris, E. E. Becklin, *Astrophys. J.* **509**, 678–686 (1998).
7. A. Boehle et al., *Astrophys. J.* **830**, 17 (2016).
8. S. Gillessen et al., *Astrophys. J.* **837**, 30 (2017).
9. R. Abuter et al., *Astron. Astrophys.* **615**, L15 (2018).

10. D. Psaltis, in *X-Ray Timing 2003: Rossi and Beyond*, P. Kaaret, F. K. Lamb, J. H. Swank, Eds. [vol. 714 of American Institute of Physics (AIP) Conference Series, AIP, 2004], pp. 29–35.
11. T. Baker, D. Psaltis, C. Skordis, *Astrophys. J.* **802**, 63 (2015).
12. P. L. Wizinowich et al., *Publ. Astron. Soc. Pac.* **118**, 297–309 (2006).
13. Materials and methods are available as supplementary materials.
14. A. M. Ghez et al., *Astrophys. J.* **689**, 1044–1062 (2008).
15. D. S. Chu et al., *Astrophys. J.* **854**, 12 (2018).
16. F. Feroz, M. P. Hobson, *Mon. Not. R. Astron. Soc.* **384**, 449–463 (2008).
17. F. Feroz, M. P. Hobson, M. Bridges, *Mon. Not. R. Astron. Soc.* **398**, 1601–1614 (2009).
18. L. I. Schiff, *Am. J. Phys.* **28**, 340–343 (1960).
19. T. Damour, A. M. Polyakov, *Gen. Relativ. Gravit.* **26**, 1171–1176 (1994).
20. S. Herrmann et al., *Phys. Rev. Lett.* **121**, 231102 (2018).
21. P. Delva et al., *Phys. Rev. Lett.* **121**, 231101 (2018).
22. G. Antoniou, A. Bakopoulos, P. Kanti, *Phys. Rev. Lett.* **120**, 131102 (2018).
23. H. O. Silva, J. Sakstein, L. Gualtieri, T. P. Sotiriou, E. Berti, *Phys. Rev. Lett.* **120**, 131104 (2018).
24. D. D. Doneva, S. S. Yazadjiev, *Phys. Rev. Lett.* **120**, 131103 (2018).
25. J. Khoury, A. Weltman, *Phys. Rev. Lett.* **93**, 171104 (2004).
26. Galactic Center Group, Orbit fitting and Scheduling Optimization Tool, Version 1.0, Zenodo (2019); 10.5281/zenodo.3305315.

ACKNOWLEDGMENTS

We thank the staff and astronomers at the W. M. Keck Observatory and the Gemini Observatory, especially G. Puniwai, J. McIlroy, S. Yeh, J. Pelletier, J. Hicock, G. Doppmann, J. Renaud-Kim, T. Ridenour, A. Hatakeyama, J. Walawender, C. Jordan, C. Wilburn, T. Stickel, H. Hershey, J. Macilroy, J. Pelletier, J. Renaud-Kim, A. Rettura, L. Rizzi, C. Alvarez, M. Lemoine-Busserolle, M. Taylor, T. Dupuy, and M. Schwamb, for their help in obtaining the new data. The W. M. Keck Observatory is operated as a scientific partnership among the California Institute of Technology, the University of California, and the National Aeronautics and Space Administration. We wish to recognize that the summit of Maunakea has always held a very important cultural role for the Indigenous Hawaiian community. We are most fortunate to have the opportunity to observe from this mountain. We thank the Subaru Telescope staff, especially Y. Minowa, T.-S. Pyo, J.-H. Kim, and E. Mieda, for their support for the Subaru observations. The Subaru Telescope is operated by the National Astronomical Observatory of Japan. **Funding:** Support for this work was provided by NSF AAG grant AST-1412615, the W. M. Keck Foundation, the Heising-Simons Foundation, the Gordon and Betty Moore Foundation, the Levine-Leichtman Family Foundation, the Preston Family Graduate Fellowship (held by A.G.), and the UCLA Galactic Center Star Society. S.J. and J.R.L. acknowledge support from NSF AAG (AST-1518273). The W. M. Keck Observatory was made possible by the generous financial support of the W. M. Keck Foundation. S.N. acknowledges financial support by JSPS KAKENHI, grants JP25707012, JP15K13463, JP18K18760, and JP19H00695. H.S. was supported by JSPS KAKENHI grants JP26610050 and JP19H01900. Y.T. was supported by JSPS KAKENHI grant JP26800150. M.T. was supported by JSPS KAKENHI grant JP17K05439 and the Daiko Foundation. W.E.K. was supported by an ESO Fellowship and the Excellence Cluster Universe, Technische Universität München. R.S. and E.G.-C. have received funding from the European Research Council under the European Union's Seventh Framework Programme (FP7/2007-2013)/ERC grant agreement 614922. R.S. acknowledges financial support from the State Agency for Research of the Spanish MCIU through the "Center of Excellence Severo Ochoa" award for the Instituto de Astrofísica de Andalucía (SEV-2017-0709). **Author contributions:** A.M.G., T.D., J.R.L., M.R.M., E.E.B., K.M., and A.H. contributed to conceptualization and design of the experiment. A.M.G., T.D., J.R.L., M.R.M., E.E.B., K.M., D.C., S.J., S.S., A.K.G., K.K.O., S.N., H.S., M.T., Y.T., R.C., Z.C., A.C., J.E.L., G.W., and S.C. made observations. T.D., D.C., S.N., S.C., and A.C., participated in reducing spectroscopic data and making RV measurements. J.R.L., S.J., S.S., A.K.G., Z.C., G.W., R.S., and E.G.-C. reduced imaging data and made astrometric measurements. A.M.G., T.D., A.H., G.D.M., J.R.L., D.C., S.J., R.S., E.G.-C., S.S., A.K.G., W.E.K., G.W., and A.Z. participated in methodology development for improving astrometric and RV

measurements. G.D.M., A.H., and T.D. participated in statistical modeling and model comparisons. K.M., R.C., P.W., and J.E.L. participated in building and improving instrumentation. All authors participated in writing and discussions of the paper. **Competing interests:** The authors declare no competing interests. **Data and materials availability:** Raw observational data are archived at the Keck Observatory Archive (<https://www2.keck.hawaii.edu/koa/public/koa.php>), the Gemini Observatory Archive (<https://archive.gemini.edu/searchform>), and the Subaru Mitaka Okayama

Kiso Archive (<https://smoka.nao.ac.jp/>) under the dates and instruments listed in tables S1 and S4. Our reduced astrometric and RV measurements are provided in data S1 and S2. The nested sampling chains are provided in data S3. Software for the orbit modeling and scheduling tool is available at Zenodo (26).

SUPPLEMENTARY MATERIALS

science.sciencemag.org/content/365/6454/664/suppl/DC1
Materials and Methods

Supplementary Text
Figs. S1 to S18
Tables S1 to S13
References (27–93)
Data S1 to S4

26 October 2018; accepted 11 July 2019
Published online 25 July 2019
10.1126/science.aav8137

Relativistic redshift of the star S0-2 orbiting the Galactic Center supermassive black hole

Tuan Do, Aurelien Hees, Andrea Ghez, Gregory D. Martinez, Devin S. Chu, Siyao Jia, Shoko Sakai, Jessica R. Lu, Abhimat K. Gautam, Kelly Kosmo O'Neil, Eric E. Becklin, Mark R. Morris, Keith Matthews, Shogo Nishiyama, Randy Campbell, Samantha Chappell, Zhuo Chen, Anna Ciurlo, Arezu Dehghanfar, Eulalia Gallego-Cano, Wolfgang E. Kerzendorf, James E. Lyke, Smadar Naoz, Hiromi Saida, Rainer Schödel, Masaaki Takahashi, Yohsuke Takamori, Gunther Witzel and Peter Wizinowich

Science **365** (6454), 664-668.

DOI: 10.1126/science.aav8137 originally published online July 25, 2019

Gravitational redshift in the Galactic Center

General relativity predicts that light emitted by an object in a strong gravitational field—for example, close to a black hole—should be shifted to longer wavelengths. This gravitational redshift does not exist in the Newtonian theory of gravity. Do *et al.* monitored the position and spectrum of the star S0-2 as it passed Sagittarius A*, the supermassive black hole at the center of the Milky Way. Around the closest part of S0-2's 16-year orbit, they detected the effect of gravitational redshift on its spectrum. These results are more consistent with general relativity than Newtonian gravity at the 5σ level.

Science, this issue p. 664

ARTICLE TOOLS

<http://science.sciencemag.org/content/365/6454/664>

SUPPLEMENTARY MATERIALS

<http://science.sciencemag.org/content/suppl/2019/07/24/science.aav8137.DC1>

REFERENCES

This article cites 87 articles, 1 of which you can access for free
<http://science.sciencemag.org/content/365/6454/664#BIBL>

PERMISSIONS

<http://www.sciencemag.org/help/reprints-and-permissions>

Use of this article is subject to the [Terms of Service](#)

Science (print ISSN 0036-8075; online ISSN 1095-9203) is published by the American Association for the Advancement of Science, 1200 New York Avenue NW, Washington, DC 20005. The title *Science* is a registered trademark of AAAS.

Copyright © 2019 The Authors, some rights reserved; exclusive licensee American Association for the Advancement of Science. No claim to original U.S. Government Works